A NEW RECONSTRUCTION METHOD FOR THE INVERSE SOURCE PROBLEM FROM PARTIAL BOUNDARY MEASUREMENTS

A. CANELAS, A. LAURAIN, AND A.A. NOVOTNY

Abstract. The inverse source problem consists in reconstructing a mass distribution in a geometrical domain from boundary measurements of the associated potential and its normal derivative. In this paper the inverse source problem is reformulated as a topology optimization problem, where the support of the mass distribution is the unknown variable. The Kohn-Vogelius functional is minimized. It measures the misfit between the solutions of two auxiliary problems containing information about the boundary measurements. The Newtonian potential is used to complement the unavailable information on the hidden boundary. The resulting topology optimization algorithm is based on an analytic formula for the variation of the Kohn-Vogelius functional with respect to a class of mass distributions consisting of a finite number of ball-shaped trial anomalies. The resulting reconstruction algorithm is non-iterative and very robust with respect to noisy data. Finally, in order to show the effectiveness of the devised reconstruction algorithm, some numerical experiments in two and three spatial dimensions are presented.

1. Introduction

The inverse source problem consists of determining the mass density distribution in a geometrical domain from boundary measurements of the associated potential and its normal derivative. It is understood here as a mathematical model used to comprehend many relevant problems in geophysics, such as the determination of the mass density inside Earth from measurements of the gravitational field. Potential applications have fueled research into new numerical algorithms of reconstruction [11]. In particular, there are mainly two applications of the inverse source problem: the reconstruction of the mass density distribution inside the whole Earth, which is done with the purpose of obtaining information of the dynamical processes taking place inside Earth; and the reconstruction of the mass density distribution of small regions of Earth, located close to its surface. This second application is particularly important in mining and engineering.

The model problem of source reconstruction we are dealing with is notoriously ill-posed [10]. In order to handle the question of uniqueness, strong assumptions, which usually do not hold, are made on the class of mass distributions to be reconstructed. For instance, it is well known that uniqueness holds in the class of mass distributions corresponding to single star-shaped anomalies [11]. The stability of the reconstruction can be obtained by introducing a regularization of the inverse operator, such as total variation techniques or Tikhonov regularization, but the numerical difficulties usually prevent the reconstruction algorithms from obtaining good results. Additional practical issues, such as partial boundary measurements, make the problem of reconstruction even more difficult.

In this paper we assume that measurements of the Newtonian potential and its normal derivative are simultaneously taken on the same part of the boundary of the domain of interest. Using these measurements, a numerical method for the source reconstruction is formulated following some of the ideas presented in [7]. In that paper the inverse problem was reformulated as a topology optimization problem, where the support of the mass distribution is the unknown variable. The method relies on the minimization of the Kohn-Vogelius functional [13], which measures the misfit between the solutions of two auxiliary problems. One of these problems contains information about the measurement of the potential, and the other one contains information about the measurement of its normal derivative. The solutions of these auxiliary problems coincide

Key words and phrases. inverse source problem, Kohn-Vogelius criterion, minimization, reconstruction method, partial boundary measurements.

once the inverse problem is solved. The resulting topology optimization algorithm is based on an analytic formula for the variation of the Kohn-Vogelius functional with respect to a class of mass distributions consisting of a finite number of ball-shaped trial anomalies. The numerical implementation of this algorithm is straightforward, and it has shown to be effective in the solution of the two-dimensional problems with complete boundary measurements.

In this paper we extend the ideas of [7] to cover the two and three spatial dimensions cases with partial boundary measurements. In [7] the case of complete boundary measurements was treated in two dimensions, but for incomplete measurements we need to modify the approach. The additional difficulty that arises from the incomplete boundary measurements is directly addressed by modifying the auxiliary problems considered in [7], where the Newtonian potential is used to complement the unavailable information on the hidden boundary. The present method remains straightforward as the one proposed in [7]. In contrast to existing approaches, it does not use a numerical continuation technique as a previous step to obtain a complete measurement on a fictitious boundary.

Important contributions in the solution of the inverse source problem have relied on the so-called point-mass methods [3, 4, 8, 15], which have been successfully applied to treat real data in geophysical problems. The proposed approach bears relation to the point-mass methods, since the effect of a ball in the boundary measurements is exactly the same as that of a point-mass of same total mass. However, our method differs from the point-mass methods in several important features. First of all, point-mass methods were designed to treat real data in geophysical problems, so that these methods use several complex and sometimes *ad hoc* procedures, whereas we consider a more idealized situation, for which we can perform a rigorous mathematical analysis. In addition, instead of using a cost functional concentrated on the boundary, the proposed approach is based on the so-called Kohn-Vogelius cost functional [14], which is defined in the whole domain. The Kohn-Vogelius functional has proved to be more stable than boundary cost functionals for several classes of inverse problems (see [14] for details). A third fundamental difference with respect to point-mass [3, 4, 8, 15] and level-set approaches [12, 16] is that the method presented here is of second-order, since we consider the second derivative with respect to topology changes, whereas existing methods are based on first-order sensitivity analysis. In our case the second derivative allows to evaluate *exactly* the variation of the cost functional with respect to the simultaneous creation of several ball-shaped anomalies, which leads to a direct and very accurate reconstruction. In fact, we show through some examples, that our method can give a precise idea of important qualitative and quantitative features of the solution to the inverse problem we are dealing with. Unlike other methods, the resulting reconstruction algorithm is non-iterative and thus very robust with respect to noisy data. In short, we claim that the idea of quantifying the effect of several ball-shaped anomalies in the Kohn-Vogelius functional by performing a second-order topological asymptotic analysis leads to a new method – substantially different to those referred above – with potential applications to other classes of inverse problems.

Admittedly, the approximation of the solution by a finite number of balls can be seen as a limitation of our approach. However, the reconstruction obtained may serve as an initial guess for other well-established and more computational intensive iterative methods [3, 6, 9, 12, 16, 20]. We emphasize that our choice of using ball-shaped trial anomalies is just a particular case of *topology optimization* techniques [18]. Actually, the analysis performed in this paper can be extended to the case of arbitrary-shaped anomalies, whereas such an extension is not possible for other available methods. This would require a more complicated asymptotic expansion, but the core idea of the algorithm would be identical. In addition, our approach could be the basis for alternative numerical methods of reconstruction, for instance using the topological derivative concept coupled with level-set methods [1]. Thus, the minimization of the Kohn-Vogelius functional by following a second-order topology optimization approach introduces a new perspective.

The paper layout goes as follows. Section 2 states the inverse source problem and formulates it as a topology optimization problem. Section 3 introduces the asymptotic expansion of the Kohn-Vogelius functional with respect to a finite number of ball-shaped trial anomalies. Section 4 describes the numerical approach and presents various examples in two and three dimensions with partial boundary measurements, showing that the proposed technique can effectively find the shape and topology of the unknown mass distribution. Some concluding remarks are drawn in the last section.

2. Problem Formulation

Let $\Omega \subset \mathbb{R}^n$ be an open and bounded domain ($n = 2, 3$), with Lipschitz boundary $\partial\Omega$. Introduce $\Gamma_M \subset \partial\Omega$ the boundary where the measurements are taken and $\Gamma = \partial\Omega \setminus \Gamma_M$ the remainder (hidden) boundary, where there is no information. Let us introduce the following boundary value problem:

$$\left\{ \begin{array}{rcll} -\Delta u & = & b^* & \text{in} \quad \Omega \,, \\ u & = & u^* \\ -\partial_n u & = & q^* \end{array} \right\} \text{on} \quad \Gamma_M \,. \tag{2.1}$$

Problem 1. *The inverse source problem reads: given $q^* \in H^{-1/2}(\Gamma_M)$ and $u^* \in H^{1/2}(\Gamma_M)$, find the unknown source $b^* \in PC_\gamma(\Omega)$ such that there exists $u[b^*] \in H^1(\Omega)$ satisfying (2.1), where*

$$PC_\gamma(\Omega) := \{ b \in L^\infty(\Omega) \ : \ b = \gamma\chi_\omega, \ \omega \subset \Omega \text{ is measurable} \} \,. \tag{2.2}$$

Here, χ_ω denotes the indicator function of the set ω and $\gamma \in \mathbb{R}$ is given. In addition, we assume that the sets ω in $PC_\gamma(\Omega)$ are of the form:

$$\omega = \bigcup_{i \in \mathcal{I}} \omega_i \quad \text{with} \quad \omega_i \cap \omega_j = \emptyset \quad \text{for} \quad i \neq j \,. \tag{2.3}$$

where $m > 0$ is a given integer, $\mathcal{I} = \{1, ..., m\}$ and each ω_i is assumed to be measurable and simply connected. See the sketch in Figure 1.

Consider a source term $b^* = \gamma\chi_{\omega^*} \in PC_\gamma(\Omega)$ and define the associated potential by

$$u[b^*](x) = \int_\Omega K(x, y) b^*(y) \, dy \,, \tag{2.4}$$

where the kernel $K(x, y)$ is given by

$$K(x, y) = \left\{ \begin{array}{ll} \dfrac{1}{4\pi|x - y|} & \text{for} \quad n = 3 \,, \\ -\dfrac{1}{2\pi} \ln|x - y| & \text{for} \quad n = 2 \,. \end{array} \right. \tag{2.5}$$

Define then

$$u^* := u[b^*]|_{\Gamma_M} \text{ and } q^* := -\partial_n u[b^*]|_{\Gamma_M} \,. \tag{2.6}$$

To address Problem 1, we propose to reformulate it as an optimization problem. The idea is to minimize the misfit between the solutions of two auxiliary problems that contain information on the boundary measurements. Since one of them uses the Dirichlet data u^* and the other one uses the Neumann data q^* as boundary conditions, then the auxiliary problems are referred to as Dirichlet and Neumann boundary value problems, respectively. In other words, we minimize the so-called Kohn-Vogelius functional [13]:

$$\min_{b \in PC_\gamma(\Omega)} J(b) := \frac{1}{2} \int_\Omega \left(u^D[b] - u^N[b] \right)^2 \,, \tag{2.7}$$

where $u^D[b]$ is solution to the Dirichlet boundary value problem

$$\left\{ \begin{array}{rcll} -\Delta u^D[b] & = & b & \text{in} \quad \Omega \,, \\ u^D[b] & = & u^* & \text{on} \quad \Gamma_M \,, \\ u^D[b] & = & u^T[b] & \text{on} \quad \Gamma \,, \end{array} \right. \tag{2.8}$$

and $u^N[b]$ is solution to the Neumann boundary value problem

$$\left\{\begin{array}{rcll} -\Delta u^N[b] &=& b & \text{in } \Omega\,, \\ -\partial_n u^N[b] &=& q^* & \text{on } \Gamma_M\,, \\ u^N[b] &=& u^T[b] & \text{on } \Gamma\,. \end{array}\right. \tag{2.9}$$

The Newtonian potential

$$u^T[b] = \int_\Omega K(x,y)b(y)\,dy\,, \tag{2.10}$$

is used to complement the information on the hidden boundary Γ. Note that the domain Ω and the part Γ of its boundary $\partial\Omega$ do not represent physical quantities and are introduced to get a meaningful mathematical model. Actually, the inverse source problem may e.g. be defined in the whole half space $\mathbb{R}^{n-1}\times(-\infty,0)$, as represented in Figure 1. The only constraint on Ω is that it has to be large enough to contain any possible anomaly, since (2.10) is correct only if this requirement is satisfied. In the following we assume that any possible anomaly is in Ω.

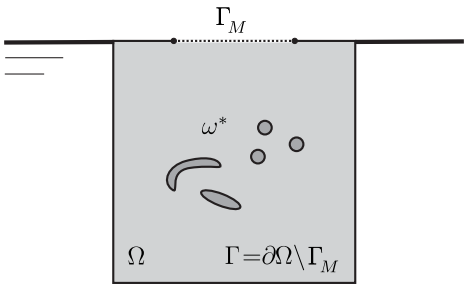

FIGURE 1. The inverse source problem.

3. Exact variation of the Kohn-Vogelius shape functional

Let us consider a perturbation of ω confined in a small set $\varpi_{\varepsilon,\widehat{x}} = \widehat{x} + \varepsilon\varpi$ of size $\varepsilon > 0$, or the union $\varpi_{\mathbf{e},\widehat{\mathbf{x}}} := \cup_{i\in\mathcal{I}}\varpi_{\varepsilon_i,\widehat{x}_i}$ of such sets, where $\mathbf{e} := \{\varepsilon_i\}_{i\in\mathcal{I}}$, $\widehat{\mathbf{x}} := \{\widehat{x}_i\}_{i\in\mathcal{I}}$. Here, $\widehat{x}_i \in \Omega$ and $\varpi \subset \mathbb{R}^n$, with $0 \in \varpi$, is fixed. We consider the particular case $\varpi_{\mathbf{e},\widehat{\mathbf{x}}} = \cup_{i\in\mathcal{I}} B(\varepsilon_i,\widehat{x}_i)$, where $B(\varepsilon_i,\widehat{x}_i)$ is a ball of radius ε_i and center $\widehat{x}_i \in \Omega$. The perturbed source term is then defined as

$$b_{\mathbf{e},\widehat{\mathbf{x}}} = b + \gamma \sum_{i\in\mathcal{I}} \chi_{B(\varepsilon_i,\widehat{x}_i)}\,. \tag{3.1}$$

where $b \in PC_\gamma(\Omega)$ is given. We are looking for an expansion of the perturbed counterpart of the Kohn-Vogelius shape functional $J(b_{\mathbf{e},\widehat{\mathbf{x}}})$ of the form [18]

$$J(b_{\mathbf{e},\widehat{\mathbf{x}}}) = J(b) + \sum_{i\in\mathcal{I}} f_1(\varepsilon_i) D^1 J(\widehat{x}_i) + \sum_{i,j\in\mathcal{I}} f_2(\varepsilon_i,\varepsilon_j) D^2 J(\widehat{x}_i,\widehat{x}_j) + \mathcal{R}(\mathbf{e},\widehat{\mathbf{x}})\,, \tag{3.2}$$

where $f_1(\varepsilon_i)$ and $f_2(\varepsilon_i,\varepsilon_j)$ are positive functions such that

$$\lim_{\varepsilon_i\to 0} f_1(\varepsilon_i) = 0, \quad \lim_{\varepsilon_i,\varepsilon_j\to 0} \frac{f_2(\varepsilon_i,\varepsilon_j)}{f_1(\varepsilon_i)} = 0 \quad \text{and} \quad \lim_{\mathbf{e}\to 0} \frac{\mathcal{R}(\mathbf{e},\widehat{\mathbf{x}})}{f_2(\varepsilon_i,\varepsilon_j)} = 0 \quad \forall i,j \in \mathcal{I}. \tag{3.3}$$

Then the functions D^1J and D^2J are called first and second order variations of J. The perturbed shape functional is written as

$$J(b_{\mathbf{e},\widehat{\mathbf{x}}}) = \frac{1}{2}\int_\Omega (u^D[b_{\mathbf{e},\widehat{\mathbf{x}}}] - u^N[b_{\mathbf{e},\widehat{\mathbf{x}}}])^2\,, \tag{3.4}$$

where $u^D[b_{\mathbf{e},\widehat{\mathbf{x}}}]$ and $u^N[b_{\mathbf{e},\widehat{\mathbf{x}}}]$ are solutions of

$$\left\{\begin{array}{rcll} -\Delta u^D[b_{\mathbf{e},\widehat{\mathbf{x}}}] &=& b_{\mathbf{e},\widehat{\mathbf{x}}} & \text{in } \Omega\,, \\ u^D[b_{\mathbf{e},\widehat{\mathbf{x}}}] &=& u^* & \text{on } \Gamma_M\,, \\ u^D[b_{\mathbf{e},\widehat{\mathbf{x}}}] &=& u^T[b_{\mathbf{e},\widehat{\mathbf{x}}}] & \text{on } \Gamma\,, \end{array}\right. \tag{3.5}$$

$$\left\{\begin{array}{rcll} -\Delta u^N[b_{\mathbf{e},\widehat{\mathbf{x}}}] &=& b_{\mathbf{e},\widehat{\mathbf{x}}} & \text{in} \quad \Omega\,, \\ -\partial_n u^N[b_{\mathbf{e},\widehat{\mathbf{x}}}] &=& q^* & \text{on} \quad \Gamma_M\,, \\ u^N[b_{\mathbf{e},\widehat{\mathbf{x}}}] &=& u^T[b_{\mathbf{e},\widehat{\mathbf{x}}}] & \text{on} \quad \Gamma\,, \end{array}\right. \tag{3.6}$$

Now, we present the derivation of the expansions for the functions $u^D[b_{\mathbf{e},\widehat{\mathbf{x}}}]$ and $u^N[b_{\mathbf{e},\widehat{\mathbf{x}}}]$. First, note that $u^T[b_{\mathbf{e},\widehat{\mathbf{x}}}]$ can be expressed as

$$\begin{aligned} u^T[b_{\mathbf{e},\widehat{\mathbf{x}}}](x) &= \int_\Omega K(x,y) b_{\mathbf{e},\widehat{\mathbf{x}}}(y)\,dy \\ &= u^T[b](x) + \gamma \sum_{i\in\mathcal{I}} \int_{B(\varepsilon_i,\widehat{x}_i)} K(x,y)\,dy\,. \end{aligned} \tag{3.7}$$

We can simplify the above expression by using some properties of the kernel $K(x,y)$, which is harmonic with respect to the variable y and does not have any singularity when $x \in \Omega \setminus \overline{B(\varepsilon_i,\widehat{x}_i)}$ and $y \in B(\varepsilon_i,\widehat{x}_i)$. According to the mean value theorem for harmonic functions we get

$$\int_{B(\varepsilon_i,\widehat{x}_i)} K(x,y)\,dy = |B(\varepsilon_i,\widehat{x}_i)| K(x,\widehat{x}_i) \quad \text{for } x \in \Omega \setminus \overline{B(\varepsilon_i,\widehat{x}_i)}\,, \tag{3.8}$$

where $|B(\varepsilon_i,\widehat{x}_i)|$ is the Lebesgue measure of the ball $B(\varepsilon_i,\widehat{x}_i)$. This yields

$$u^T[b_{\mathbf{e},\widehat{\mathbf{x}}}](x) = u^T[b](x) + \gamma \sum_{i\in\mathcal{I}} |B(\varepsilon_i,\widehat{x}_i)| K(x,\widehat{x}_i)\,. \tag{3.9}$$

The function $u^D[b_{\mathbf{e},\widehat{\mathbf{x}}}]$ can be expressed as

$$u^D[b_{\mathbf{e},\widehat{\mathbf{x}}}](x) = u^D[b](x) + \sum_{i\in\mathcal{I}} |B(\varepsilon_i,\widehat{x}_i)| v_{\varepsilon_i}(x)\,, \tag{3.10}$$

where each function v_{ε_i} is solution to

$$\left\{\begin{array}{rcll} -\Delta v_{\varepsilon_i} &=& \dfrac{\gamma}{|B(\varepsilon_i,\widehat{x}_i)|}\,\chi_{B(\varepsilon_i,\widehat{x}_i)} & \text{in} \quad \Omega\,, \\ v_{\varepsilon_i} &=& 0 & \text{on} \quad \Gamma_M\,. \\ v_{\varepsilon_i} &=& \gamma K(x,\widehat{x}_i) & \text{on} \quad \Gamma\,. \end{array}\right. \tag{3.11}$$

One may express v_{ε_i} as a sum of the form $v_{\varepsilon_i} = v^p_{\varepsilon_i} + v^q_{\varepsilon_i}$, where $v^p_{\varepsilon_i}$ is a particular solution obtained by using the fundamental solution of the Laplacian, namely:

$$v^p_{\varepsilon_i}(x) = \frac{\gamma}{|B(\varepsilon_i,\widehat{x}_i)|} \int_{B(\varepsilon_i,\widehat{x}_i)} K(x,y)\,dy\,, \tag{3.12}$$

which, according to (3.8), satisfies

$$v^p_{\varepsilon_i}(x) = \gamma K(x,\widehat{x}_i) \quad \text{for } x \in \Omega \setminus \overline{B(\varepsilon_i,\widehat{x}_i)}\,, \tag{3.13}$$

so that the remainder $v^q_{\varepsilon_i} := v_{\varepsilon_i} - v^p_{\varepsilon_i}$, which is used to compensate the discrepancy left by $v^p_{\varepsilon_i}$ on $\partial\Omega$, is harmonic and solves the homogeneous boundary value problem:

$$\left\{\begin{array}{rcll} -\Delta v^q_{\varepsilon_i} &=& 0 & \text{in} \quad \Omega\,, \\ v^q_{\varepsilon_i} &=& -v^p_{\varepsilon_i} & \text{on} \quad \Gamma_M\,. \\ v^q_{\varepsilon_i} &=& 0 & \text{on} \quad \Gamma\,. \end{array}\right. \tag{3.14}$$

Note that from (3.13), $v^p_{\varepsilon_i}(x)$ actually does not depend on ε_i for $x \in \Omega \setminus \overline{B(\varepsilon_i,\widehat{x}_i)}$. Then, from (3.14) we observe that $v^q_{\varepsilon_i}$ also does not depend on ε_i and since $v_{\varepsilon_i} = v^p_{\varepsilon_i} + v^q_{\varepsilon_i}$ we have that $v_{\varepsilon_i}(x)$ is also independent of ε_i for $x \in \Omega \setminus \overline{B(\varepsilon_i,\widehat{x}_i)}$.

For the function $u^N[b_{\mathbf{e},\widehat{\mathbf{x}}}]$ we introduce the expansion:

$$u^N[b_{\mathbf{e},\widehat{\mathbf{x}}}](x) = u^N[b](x) + \sum_{i\in\mathcal{I}} |B(\varepsilon_i,\widehat{x}_i)|(v_{\varepsilon_i}(x) + h_i(x))\,, \tag{3.15}$$

with function h_i solution to

$$\left\{\begin{array}{rcll} -\Delta h_i &=& 0 & \text{in} \quad \Omega\,, \\ -\partial_n h_i &=& g_i & \text{on} \quad \Gamma_M\,, \\ h_i &=& 0 & \text{on} \quad \Gamma\,, \end{array}\right. \tag{3.16}$$

where $g_i = \partial_n v_{\varepsilon_i}$ on Γ_M is actually independent of ε_i according to the previous comments, with v_{ε_i} solution to (3.11).

Finally, after introducing the notation $a_i := |B(\varepsilon_i, \widehat{x}_i)|$, the expansion of the Kohn-Vogelius criterion reads using (3.10) and (3.15):

$$\begin{aligned} J(b_{\mathbf{e},\widehat{\mathbf{x}}}) &= \frac{1}{2}\int_\Omega \left(u^D[b_{\mathbf{e},\widehat{\mathbf{x}}}] - u^N[b_{\mathbf{e},\widehat{\mathbf{x}}}]\right)^2 \\ &= \frac{1}{2}\int_\Omega \left[u^D[b] + \sum_{i\in\mathcal{I}} a_i v_{\varepsilon_i} - \left(u^N[b] + \sum_{i\in\mathcal{I}} a_i(v_{\varepsilon_i} + h_i)\right)\right]^2 \\ &= \frac{1}{2}\int_\Omega \left[(u^D[b] - u^N[b]) - \sum_{i\in\mathcal{I}} a_i h_i\right]^2 \\ &= J(b) - \int_\Omega (u^D[b] - u^N[b]) \sum_{i\in\mathcal{I}} a_i h_i + \frac{1}{2}\int_\Omega \left(\sum_{i\in\mathcal{I}} a_i h_i\right)^2 . \end{aligned} \tag{3.17}$$

In particular, we can state the following result:

Proposition 2. *The closed formula for the variation of the Kohn-Vogelius shape functional with respect to a class of finite number of ball-shaped trial anomalies is given by*

$$J(b_{\mathbf{e},\widehat{\mathbf{x}}}) = J(b) - \int_\Omega (u^D[b] - u^N[b]) \sum_{i\in\mathcal{I}} a_i h_i + \frac{1}{2}\int_\Omega \left(\sum_{i\in\mathcal{I}} a_i h_i\right)^2 . \tag{3.18}$$

Therefore, from (3.2) *we have* $f_1(a_i) = a_i$, $f_2(a_i, a_j) = \frac{1}{2}a_i a_j$ *and* $\mathcal{R}(\mathbf{e}, \widehat{\mathbf{x}}) \equiv 0$. *In addition,*

$$D^1 J(\widehat{x}_i) = \int_\Omega (u^D[b] - u^N[b]) h_i \quad \textit{and} \quad D^2 J(\widehat{x}_i, \widehat{x}_j) = \int_\Omega h_i h_j \, . \tag{3.19}$$

Remark 3. *Note that* h_i *depends on* $\widehat{x}_i$ *through the boundary data* g_i *in problem* (3.16)*, since it also depends on* $\widehat{x}_i$ *through the source term in* (3.11)*. Consequently,* (3.11) *and* (3.16) *must be solved for each* $\widehat{x}_i$ *in order to evaluate the expansion of* J *at* $\widehat{x}_i$*. However, the solutions of these auxiliary problems do not depend on the given source* b*, so that they can be solved once before the reconstruction process and the values for* h_i *and* $D^2 J(\widehat{x}_i, \widehat{x}_j)$ *can be tabulated. Therefore, during the reconstruction process only* $D^1 J(\widehat{x}_i)$ *has to be calculated, which implies the solution of only the two auxiliary problems for* u^D *and* u^N*, respectively depending on the boundary data* u^* *and* q^**.*

4. Numerical results

When using perturbations of the form $\varpi_{\mathbf{e},\widehat{\mathbf{x}}} = \cup_{i\in\mathcal{I}} B(\varepsilon_i, \widehat{x}_i)$, the shape optimization problem (2.7) reduces to the minimization of $J(b_{\mathbf{e},\widehat{\mathbf{x}}})$ with respect to $\mathbf{e}$ and $\widehat{\mathbf{x}}$. We introduce the change of variables $a_i := |B(\varepsilon_i, \widehat{x}_i)|$, $i \in \mathcal{I}$ and $\mathbf{a} := \{a_i\}_{i\in\mathcal{I}}$. For a fixed point $\widehat{\mathbf{x}}$ we look for the areas minimizing $J_{\widehat{\mathbf{x}}}(\mathbf{a}) := J(b_{\mathbf{e},\widehat{\mathbf{x}}})$. The following proposition shows the convenience of this approach:

Proposition 4. *The function* $J_{\widehat{\mathbf{x}}}(\mathbf{a})$ *is a convex quadratic function of the variable* $\mathbf{a}$*. In addition, if the functions* $\{h_i\}_{i\in\mathcal{I}}$*, solutions to* (3.16) *for the points* $\{\widehat{x}_i\}_{i\in\mathcal{I}}$ *are linearly independent, then* $J_{\widehat{\mathbf{x}}}(\mathbf{a})$ *is a strictly convex quadratic function.*

Proof. These results follow from Proposition 2, Theorems 3.3.7 and 3.3.8 in [5]. In effect, from Proposition 2 we have

$$J_{\widehat{\mathbf{x}}}(\mathbf{a}) = J_{\widehat{\mathbf{x}}}(\mathbf{0}) + \sum_{i\in\mathcal{I}} a_i D^1 J(\widehat{x}_i) + \frac{1}{2}\sum_{i,j\in\mathcal{I}} a_i a_j D^2 J(\widehat{x}_i, \widehat{x}_j) \, , \tag{4.1}$$

then, the Hessian matrix of $J_{\widehat{\mathbf{x}}}(\mathbf{a})$ has components $D^2J(\widehat{x}_i,\widehat{x}_j)$. This matrix is positive semidefinite since, from (3.19):

$$\sum_{i,j\in\mathcal{I}} D^2J(\widehat{x}_i,\widehat{x}_j)a_ia_j = \int_\Omega \left(\sum_{i\in\mathcal{I}} a_ih_i\right)^2 \geq 0\ , \tag{4.2}$$

and is positive definite if the functions $\{h_i\}_{i\in\mathcal{I}}$ are linearly independent, since in this case the sum is zero only if $\mathbf{a}=\mathbf{0}$. □

To find the optimal $\mathbf{a}$ we differentiate (4.1) with respect to a_i to obtain the first order optimality conditions:

$$\sum_{j\in\mathcal{I}} D^2J(\widehat{x}_i,\widehat{x}_j)a_j = -D^1J(\widehat{x}_i) \quad \text{for} \quad i\in\mathcal{I}\ , \tag{4.3}$$

where $D^1J(\widehat{x}_i)$ and $D^2J(\widehat{x}_i,\widehat{x}_j)$ are given by (3.19). Note that from Proposition 4, the matrix of the linear system (4.3) is always positive semidefinite and becomes positive definite if the functions $\{h_i\}_{i\in\mathcal{I}}$ are linearly independent. In this last case, the solution to (4.3) always exists, and is the unique global minimum of $J_{\widehat{\mathbf{x}}}(\mathbf{a})$.

Denote $\mathbf{M}=\{M_{ij}\}_{i,j\in\mathcal{I}^2}$ the matrix with coefficients $M_{ij}=D^2J(\widehat{x}_i,\widehat{x}_j)$ and $\mathbf{v}=\{v_i\}_{i\in\mathcal{I}}$, with $v_i=D^1J(\widehat{x}_i)$. Then (4.3) is equivalent to

$$\mathbf{Ma}=-\mathbf{v}\ . \tag{4.4}$$

Assume that $\mathbf{M}$ is invertible, then the solution to (4.4) is $\mathbf{a}^\star=-\mathbf{M}^{-1}\mathbf{v}$.

We say that the point $\widehat{\mathbf{x}}=\{\widehat{x}_i\}_{i\in\mathcal{I}}$ is feasible if (4.3) has a meaningful solution in the sense that $a_i>0$, $i\in\mathcal{I}$. The numerical practice shows us that it is not necessary to consider additional constraints to avoid the overlapping between different balls or to have $\varpi_{\mathbf{e},\widehat{\mathbf{x}}}\subset\Omega$. Meaningful solutions are found by imposing the positivity requirement only.

After solving the linear system (4.4), we have to optimize $J_{\widehat{\mathbf{x}}}(\mathbf{a}^\star)$ with respect to $\widehat{\mathbf{x}}$ in a certain set of feasible points. Equation (4.1) can also be written as

$$J_{\widehat{\mathbf{x}}}(\mathbf{a}) = J_{\widehat{\mathbf{x}}}(\mathbf{0}) + \mathbf{v}\cdot\mathbf{a} + \frac{1}{2}\mathbf{a}\cdot\mathbf{Ma}\ , \tag{4.5}$$

Now using (4.4) and since $\mathbf{M}$ is symmetric we get

$$\begin{aligned} J_{\widehat{\mathbf{x}}}(\mathbf{a}^\star) &= J_{\widehat{\mathbf{x}}}(\mathbf{0}) + \frac{1}{2}\mathbf{v}\cdot\mathbf{a}^\star \\ &= J_{\widehat{\mathbf{x}}}(\mathbf{0}) - \frac{1}{2}\mathbf{v}\cdot\mathbf{M}^{-1}\mathbf{v}\ . \end{aligned} \tag{4.6}$$

Then the optimum $\widehat{\mathbf{x}}$, denoted as $\widehat{\mathbf{x}}^\star$, can be easily retrieved through the above formula, namely

$$\widehat{\mathbf{x}}^\star := \arg\min_{\widehat{\mathbf{x}}\in\mathbf{X}} J_{\widehat{\mathbf{x}}}(\mathbf{a}^\star)\ , \tag{4.7}$$

where $\mathbf{X}$ is the set of feasible points $\widehat{\mathbf{x}}=\{\widehat{x}_i\}_{i\in\mathcal{I}}$, with $\widehat{x}_i\in\Omega$ for each $i\in\mathcal{I}$. Here, an exhaustive search in the set $\mathbf{X}$ is performed to find the optimal $\widehat{\mathbf{x}}^\star$. Thus, due to the computational complexity of such a procedure, it is doable only if the number of balls m is small, and other algorithms for combinatorial optimization problems should be used to deal with a large m.

The next two propositions refer to the question of uniqueness of the solution of the inverse source problem in the class of sources composed by a finite number of balls. Proposition 5 gives a response in the very specific situation where the domain is a circle or a sphere, and complete boundary measurements are available. It shows that in this case the Kohn-Vogelius functional can have only one minimum. Proposition 6 considers any bounded simply-connected domain, and the possibility of having incomplete measurement of the normal derivative. However, it is valid only in the two-dimensional case, and needs a complete boundary measurement of the potential.

Proposition 5. *Consider the domain* $\Omega = \{x \in \mathbb{R}^\alpha \mid \|x\| < R\}$ *with* $\alpha = 2$ *or* $\alpha = 3$. *Then, for the case with complete boundary measurements, the minimum of the Kohn-Vogelius functional* (3.4) *in the class*

$$A := \left\{ b_{\mathbf{e},\widehat{\mathbf{x}}} = \gamma \sum_{i=1}^{n} \chi_{B(\varepsilon_i,\widehat{x}_i)}\,, n \in \mathbb{N},\ \widehat{x}_i \neq \widehat{x}_j \text{ for } i \neq j, \text{ and } \varpi_{\mathbf{e},\widehat{\mathbf{x}}} \subset \Omega \right\}, \tag{4.8}$$

is unique. In particular, Problem (2.7) *can have at most one solution in A.*

Proof. The proof is based on Proposition 4 and the linear independence of the functions h_i which, in the case of the disk or the sphere, can be obtained analytically, see [7] and Section 4.1. The proof for the two-dimensional case is given in [7]. For the three-dimensional case the proof is completely analogous. □

Proposition 6. *Consider a bounded simply-connected two-dimensional domain* $\Omega \subset \mathbb{R}^2$. *Assume we have a complete measurement* $u^* \in H^{1/2}(\partial\Omega)$, *and a measurement* $q^* \in H^{-1/2}(\Gamma_M)$. *Then, a source* b^* *in the class A of Proposition 5 such that there exists* $u \in H^1(\Omega)$ *satisfying*

$$\left\{ \begin{array}{rcll} -\Delta u &=& b^* & \text{in } \Omega\,, \\ u &=& u^* & \text{on } \partial\Omega\,, \\ -\partial_n u &=& q^* & \text{on } \Gamma_M\,. \end{array} \right. \tag{4.9}$$

is unique.

Proof. Assume $b^j \in A$ with $j = 1, 2$ are solutions of the inverse problem and that u^j are the corresponding solutions to the problems:

$$\left\{ \begin{array}{rcll} -\Delta u^j &=& b^j & \text{in } \Omega\,, \\ u^j &=& u^* & \text{on } \partial\Omega\,, \\ -\partial_n u^j &=& q^* & \text{on } \Gamma_M\,. \end{array} \right. \tag{4.10}$$

Then, the difference $w = u^2 - u^1$ solves the problem:

$$\left\{ \begin{array}{rcll} -\Delta w &=& \displaystyle\sum_{i=1}^{m} \beta_i\, \chi_{B(\varepsilon_i,\widehat{x}_i)} & \text{in } \Omega\,, \\ w &=& 0 & \text{on } \partial\Omega\,, \\ -\partial_n w &=& 0 & \text{on } \Gamma_M\,, \end{array} \right. \tag{4.11}$$

for some m, $\beta_i, \varepsilon_i \in \mathbb{R}$ and $\widehat{x}_i \in \mathbb{R}^2$, $i = 1, ..., m$, defined implicitly by (4.11), where the numbers β_i, $i = 1, ..., m$, are not required to be positive. In the two-dimensional case, by using the Riemann mapping theorem and the Poisson integral, we can always construct functions f^j, $j = 1, ..., m$, satisfying

$$\left\{ \begin{array}{rcll} -\Delta f^j &=& 0 & \text{in } \Omega\,, \\ f^j &=& 0 & \text{on } \partial\Omega \setminus \Gamma_M\,, \\ f^j(\widehat{x}_i) &=& \delta_{ij}\,, & \end{array} \right. \tag{4.12}$$

where δ_{ij} is the Kronecker delta, see [19]. By applying the second Green identity to w and f^j we have:

$$\int_\Omega f^j \Delta w = 0\,. \tag{4.13}$$

Since f^j are harmonic, the mean value theorem of harmonic functions gives

$$\int_\Omega f^j \Delta w = \sum_{i=1}^{m} f^j(\widehat{x}_i)\beta_i |B(\varepsilon_i, \widehat{x}_i)| = \beta_j |B(\varepsilon_j, \widehat{x}_j)| = 0\,. \tag{4.14}$$

Then $\Delta w = 0$, so that $b_1 = b_2$. □

4.1. **Example with a closed-form solution.** Let us consider the sphere $\Omega = \{x \in \mathbb{R}^3 \,:\, \|x\| < R\}$, in the case of complete boundary measurements, i.e. $\Gamma_M = \partial\Omega$. In this case problem (3.16) has only Neumann boundary conditions, so that the field equation of (3.16) must be changed to $-\Delta h_i = -\gamma/(2\pi R^3)$ and the constraint $\int_\Omega h_i = 0$ must be introduced, see [7].

Consider a generic point $\widehat{x}_i$. We introduce a spherical coordinate system so that a generic point x has coordinates (r, θ, φ), and it is oriented in such a way that $\widehat{x}_i$ has coordinates $(\widehat{r}_i, \widehat{\theta}_i = 0, \widehat{\varphi}_i = 0)$ with $0 < \widehat{r}_i < R$. Let $\widetilde{x}_i$ be the point of polar coordinates $(\widetilde{r}_i, \widetilde{\theta}_i = 0, \widetilde{\varphi}_i = 0)$ with $\widetilde{r}_i = R^2/\widehat{r}_i$. We define the functions $\widehat{s}_i(x) = \|x - \widehat{x}_i\|$, and $\widetilde{s}_i(x) = \|x - \widetilde{x}_i\|$. Note that for a generic point $x \in \partial\Omega$ of coordinates (R, θ, φ) we have

$$\left.\frac{1}{\widehat{s}_i}\right|_{r=R} = \frac{1}{\sqrt{R^2 + \widehat{r}_i^2 - 2\widehat{r}_i R\cos(\theta)}} = \frac{\widetilde{r}_i/R}{\sqrt{R^2 + \widetilde{r}_i^2 - 2\widetilde{r}_i R\cos(\theta)}} = \left.\frac{\widetilde{r}_i}{R\widetilde{s}_i}\right|_{r=R}, \tag{4.15}$$

so that it is easy to verify by direct differentiation that a solution to (3.11) for a perturbation of radius ε_i and center $\widehat{x}_i$ is

$$v_{\varepsilon_i} = \begin{cases} \dfrac{\gamma}{4\pi}\left[\dfrac{3\varepsilon_i^2 - \widehat{s}_i^2}{2\varepsilon_i^3} - \dfrac{\widetilde{r}_i}{R\widetilde{s}_i}\right] & \text{in} \quad B(\varepsilon_i, \widehat{x}_i)\,, \\ \dfrac{\gamma}{4\pi}\left[\dfrac{1}{\widetilde{s}_i} - \dfrac{\widetilde{r}_i}{R\widetilde{s}_i}\right] & \text{in} \quad \Omega \setminus \overline{B(\varepsilon_i, \widehat{x}_i)}\,. \end{cases} \tag{4.16}$$

From this expression we have

$$\partial_n v_{\varepsilon_i} = -\frac{\gamma}{4\pi}\left[\frac{R^2 - \widehat{r}_i^2}{R\widehat{s}_i^3}\right]_{r=R} \quad \text{on} \quad \partial\Omega\,. \tag{4.17}$$

To obtain h_i we consider the following useful formula [2, Chap. 12]:

$$\left[R^2 + \widehat{r}_i^2 - 2\widehat{r}_i R\cos(\theta)\right]^{-1/2} = \frac{1}{R}\sum_{\ell=0}^{\infty}\left(\frac{\widehat{r}_i}{R}\right)^\ell P_\ell(\cos(\theta))\,, \tag{4.18}$$

where

$$P_\ell(t) = \frac{1}{2^\ell \ell!}\frac{d^\ell}{dt^\ell}\left[(t^2 - 1)^\ell\right],$$

are the Legendre polynomials, which satisfy the following orthogonality property [2, Chap. 12]:

$$\int_0^\pi \sin(\theta) P_\ell(\cos(\theta)) P_k(\cos(\theta))\, d\theta = \frac{2}{2\ell + 1}\delta_{\ell k}\,, \tag{4.19}$$

with $\delta_{\ell k}$ being the Kronecker delta. In addition, we have

$$\int_0^{2\pi} P_\ell(\cos(\theta)\cos(\phi) + \sin(\theta)\sin(\phi)\cos(\varphi))\, d\varphi = 2\pi P_\ell(\cos(\theta)) P_\ell(\cos(\phi))\,. \tag{4.20}$$

By considering (4.15) and (4.18), we have that the harmonic function $\widetilde{r}_i/(R\widetilde{s}_i)$ can be expressed as:

$$\frac{\widetilde{r}_i}{R\widetilde{s}_i} = \frac{1}{R}\sum_{\ell=0}^{\infty}\left(\frac{\widehat{r}_i}{R}\right)^\ell\left(\frac{r}{R}\right)^\ell P_\ell(\cos(\theta)) \quad \text{in} \quad \Omega\,. \tag{4.21}$$

Let us assume that the function h_i has the following form:

$$h_i = \frac{\gamma}{4\pi}\left[\frac{r^2}{2R^3} + \frac{A\widetilde{r}_i}{R\widetilde{s}_i} + \frac{1}{R}\sum_{\ell=0}^{\infty} A_\ell\left(\frac{r}{R}\right)^\ell P_\ell(\cos(\theta))\right] \quad \text{in} \quad \Omega\,. \tag{4.22}$$

where the real parameters A and A_ℓ, $\ell \in \mathbb{N}$ have to be determined in order to have h_i solution to (3.16), with $-\Delta h_i = -\gamma/(2\pi R^3)$.

By differentiating the previous equation, using (4.15), (4.17), and $\widetilde{r}_i = R^2/\widehat{r}_i$, we have

$$\partial_n h_i + \partial_n v_{\varepsilon_i} = \frac{\gamma}{4\pi}\left[-\frac{R^2 + (A-1)\widehat{r}_i^2 - A\widehat{r}_i R\cos(\theta)}{R\widehat{s}_i^3} + \frac{1}{R^2} + \frac{1}{R^2}\sum_{\ell=1}^{\infty}\ell A_\ell P_\ell(\cos(\theta))\right]_{r=R}, \tag{4.23}$$

which, taking $A = 2$ reduces to

$$\partial_n h_i + \partial_n v_{\varepsilon_i} = \frac{\gamma}{4\pi}\left[-\frac{1}{R\widehat{s}_i} + \frac{1}{R^2} + \frac{1}{R^2}\sum_{\ell=1}^{\infty} \ell A_\ell P_\ell(\cos(\theta))\right]_{r=R} . \tag{4.24}$$

Then, after taking into account (4.15) and the expansion (4.18), we have that the boundary condition in (3.16) is satisfied provided $\ell A_\ell = (\widehat{r}_i/R)^\ell$ for each $\ell \geq 1$. The parameter A_0 can be defined to obtain $\int_\Omega P_0(\cos(\theta))h_i = \int_\Omega h_i = 0$. In fact, by replacing the expansion (4.18) in (4.22), and by using the orthogonality property (4.19) we easily obtain $A_0 = -23/10$. Therefore, the solution to (3.16) with $-\Delta h_i = -\gamma/(2\pi R^3)$ is:

$$h_i = \frac{\gamma}{4\pi}\left[\frac{r^2}{2R^3} + \frac{2\widetilde{r}_i}{R\widetilde{s}_i} - \frac{23}{10R} + \frac{1}{R}\sum_{\ell=1}^{\infty}\frac{1}{\ell}\left(\frac{\widehat{r}_i}{R}\right)^\ell\left(\frac{r}{R}\right)^\ell P_\ell(\cos(\theta))\right] \quad \text{in} \quad \Omega\,. \tag{4.25}$$

It is also interesting to note that after differentiating the previous equation and comparing with (4.17) we obtain a formula similar to (4.18):

$$\left[R^2 + \widehat{r}_i^2 - 2\widehat{r}_i R\cos(\theta)\right]^{-3/2} = \frac{1}{R(R^2-\widehat{r}_i^2)}\sum_{\ell=0}^{\infty}(1+2\ell)\left(\frac{\widehat{r}_i}{R}\right)^\ell P_\ell(\cos(\theta))\,. \tag{4.26}$$

To obtain a better expression for h_i, consider the function f defined as

$$f = \frac{1}{R}\sum_{\ell=1}^{\infty}\frac{1}{\ell}\left(\frac{\widehat{r}_i}{R}\right)^\ell\left(\frac{r}{R}\right)^\ell P_\ell(\cos(\theta))\,. \tag{4.27}$$

By differentiating this expression with respect to r, and considering (4.21) we have

$$r\frac{\partial f}{\partial r} + \frac{1}{R} = \frac{1}{R}\sum_{\ell=0}^{\infty}\left(\frac{\widehat{r}_i}{R}\right)^\ell\left(\frac{r}{R}\right)^\ell P_\ell(\cos(\theta)) = \frac{\widetilde{r}_i}{R\widetilde{s}_i}\,. \tag{4.28}$$

From (4.27) we have $f(r=0,\theta) = 0$, then from the previous equation we obtain

$$f = \int_0^r \frac{\widetilde{r}_i - \widetilde{s}_i}{rR\widetilde{s}_i}\,dr = -\frac{1}{R}\log\left(\frac{\widetilde{r}_i + \widetilde{s}_i - r\cos\theta}{2\widetilde{r}_i}\right)\,. \tag{4.29}$$

By replacing the previous result in (4.25) we have

$$h_i = \frac{\gamma}{4\pi}\left[\frac{r^2}{2R^3} + \frac{2\widetilde{r}_i}{R\widetilde{s}_i} - \frac{23}{10R} - \frac{1}{R}\log\left(\frac{\widetilde{r}_i + \widetilde{s}_i - r\cos(\theta)}{2\widetilde{r}_i}\right)\right] \quad \text{in} \quad \Omega\,. \tag{4.30}$$

Consider another point $\widehat{x}_j$, and denote ϕ_{ij} the central angle $\widehat{x}_i O \widehat{x}_j$ where O is the center of Ω. We can orient the spherical coordinate system in such a way that $\widehat{x}_j$ has coordinates $(\widehat{r}_j, \theta = \phi_{ij}, \varphi = 0)$. The function h_j is given by (4.25) or (4.30), with the subscript 'j' instead of 'i' and the angle θ', satisfying $\cos(\theta') = \cos(\theta)\cos(\phi_{ij}) + \sin(\theta)\sin(\phi_{ij})\cos(\varphi)$, instead of θ. The second order derivatives can be obtained using (3.19), (4.21), (4.25), and the identities (4.19)–(4.20):

$$D^2 J(\widehat{x}_i, \widehat{x}_j) = \frac{\gamma^2 R}{4\pi}\left[\frac{1}{175} + \sum_{\ell=1}^{\infty}\frac{2\ell+1}{\ell^2(2\ell+3)}\left(\frac{\widehat{r}_i\widehat{r}_j}{R^2}\right)^\ell P_\ell(\cos(\phi_{ij}))\right]. \tag{4.31}$$

This last expression can be simplified further in the case $\widehat{x}_j \equiv \widehat{x}_i$ by using the Symbolic Math Toolbox of MATLAB. This gives for $t = \widehat{r}_i/R$:

$$D^2 J(\widehat{x}_i, \widehat{x}_i) = \frac{\gamma^2 R}{36\pi}\left[\frac{1427}{525} + 3\,\mathrm{dilog}(1-t^2) - 4\log(1-t^2) - \frac{8}{t^3}\,\mathrm{atanh}(t) + \frac{8}{t^2}\right]. \tag{4.32}$$

4.2. **Examples in two spacial dimensions.** In this section we present some numerical experiments in two spacial dimensions by setting $n = 2$ in the obtained formulas. In the examples we take $\Omega = (0,1) \times (0,1)$ and $\gamma = 1$, except the last one where the lack of uniqueness with respect to γ is discussed. Since we are dealing with partial boundary measurements, the observed boundary Γ_M is represented by a dashed line. The domain Ω is discretized with three-node finite elements. The mesh is generated from a grid of size 100×100, where each resulting square is divided into four triangles, leading to 40×10^3 elements. A fixed subgrid with 20×20 nodes is introduced, which is used to evaluate $D^1 J(\widehat{x}_i)$ and $D^2 J(\widehat{x}_i, \widehat{x}_j)$. This choice has been shown to be a good compromise between resolution and computational cost [7].

4.2.1. *Example 1: Partial boundary measurements, noiseless data.* In this first example, we consider the sensitivity of the reconstruction with respect to a partial boundary measurements. For a fixed target, we set different Γ_M. The target is shown in Fig. 2. The obtained results for $|\Gamma_M| = \{1.0, 0.4, 0.2, 0.1\}$ are presented in Figs. 3(a)-(d), respectively. In all cases the reconstructions match precisely the targets, even when there is very few information available.

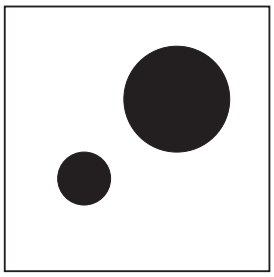

FIGURE 2. Example 1: true source term.

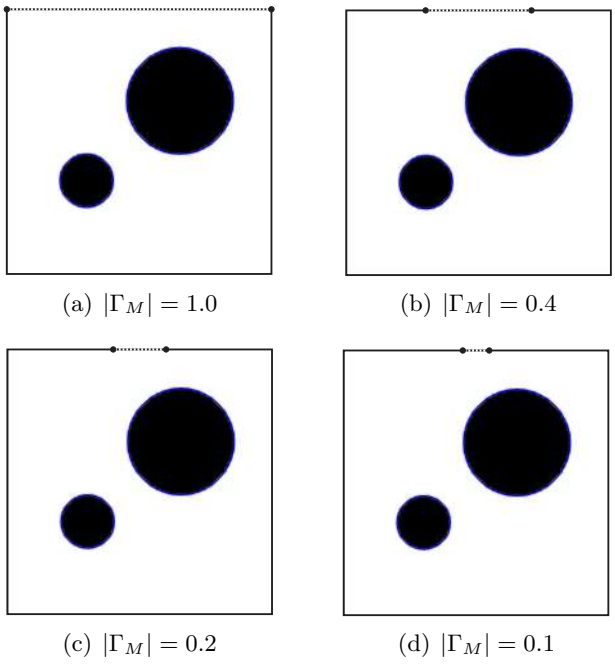

(a) $|\Gamma_M| = 1.0$ (b) $|\Gamma_M| = 0.4$

(c) $|\Gamma_M| = 0.2$ (d) $|\Gamma_M| = 0.1$

FIGURE 3. Example 1: reconstructions for different Γ_M.

4.2.2. *Example 2: Partial boundary measurements, noisy data.* The first example is revisited, but the data is corrupted with noise. In order to obtain noisy synthetic data, the true source term b^* is corrupted with white Gaussian noise of zero mean and 0.2 of standard deviation, as shown

in Fig. 4. The obtained results for $|\Gamma_M| = \{1.0, 0.4, 0.2, 0.1\}$ are presented in Figs. 5(a)-(d), respectively. Now, we observe that the less information available, the worst is the reconstruction.

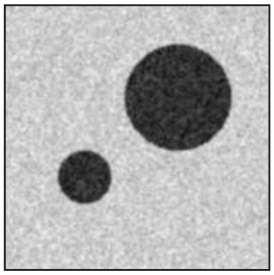

FIGURE 4. Example 2: noisy source term.

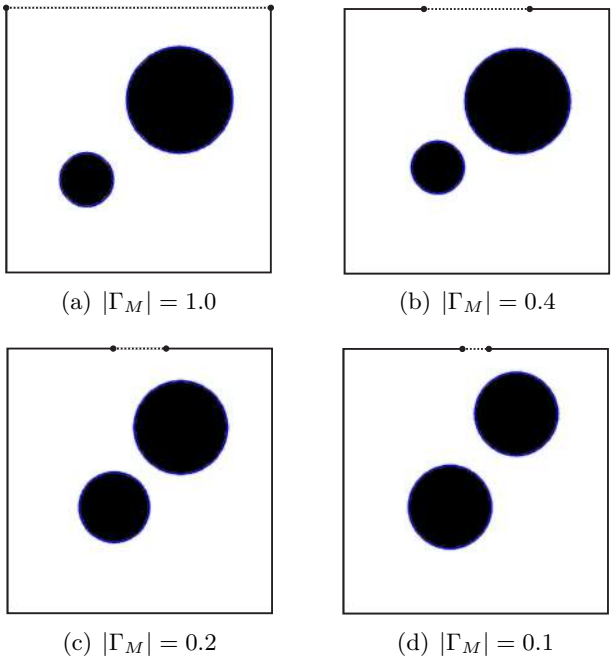

(a) $|\Gamma_M| = 1.0$ (b) $|\Gamma_M| = 0.4$

(c) $|\Gamma_M| = 0.2$ (d) $|\Gamma_M| = 0.1$

FIGURE 5. Example 2: reconstructions for different Γ_M.

4.2.3. *Example 3: Hidden anomaly.* Let us reconstruct again two anomalies, when one of them is complete hidden by the other one. The target and the obtained result for $|\Gamma_M| = 0.1$ are shown in Fig. 6. Again, the reconstruction matches precisely the target. Note that there is very few information available.

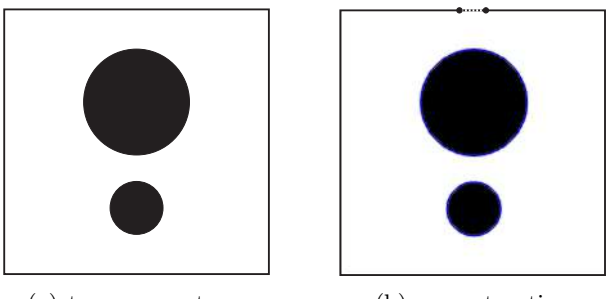

(a) true source term (b) reconstruction

FIGURE 6. Example 3: hidden anomaly.

4.2.4. *Example 4: Probing for the number of anomalies.* Now we suppose that the number of anomalies is unknown and proceed with successive trials to find the correct number of balls. We start with one trial ball and increment the number of balls every step until the algorithm provides the same result from one iteration to the next. In particular, we are looking for three anomalies, as shown in Fig. 7. The obtained results considering $|\Gamma_M| = 1.0$ for one, two, three and four trial balls are shown in Fig. 8. We note that the results obtained with three and four balls are the same up to a (very) small fourth trial ball (Fig. 8(d)), allowing us to conclude that there are only three main anomalies, which corroborates with the target we are reconstructing (Fig. 7). Therefore, such a problem can be solved in one shot by supposing that the number $m > m^*$, with m^* used to denote the actual number of anomalies, is a priori known.

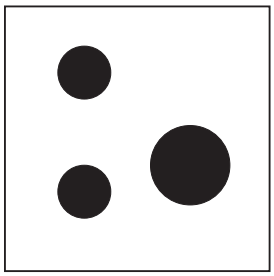

FIGURE 7. Example 4: true source term.

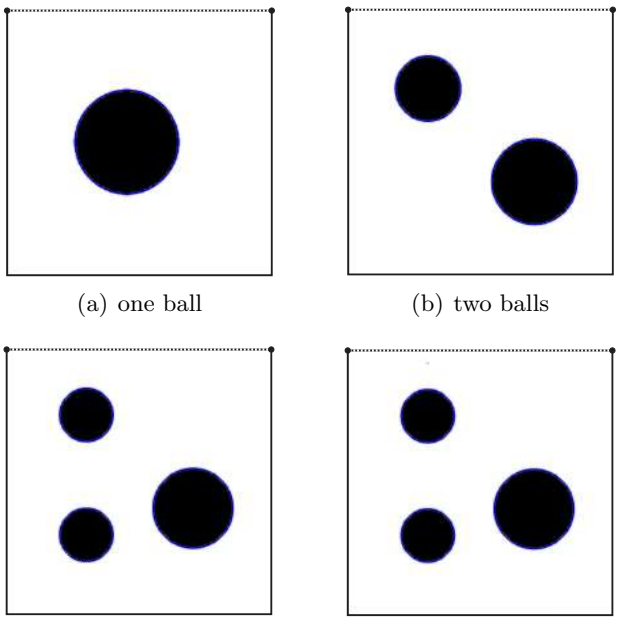

(a) one ball (b) two balls

(c) three balls (d) four balls

FIGURE 8. Example 4: looking for three anomalies.

4.2.5. *Example 5: Shape and topology reconstruction.* In this example we detect the topology as well as the shape of the anomalies. In particular, we approximate an L-shaped anomaly and a circular one by four balls considering $|\Gamma_M| = 1.0$, as shown in Fig. 9. Through this example, we show that the proposed method is able to reconstruct approximately the shape and the topology of the mass distribution from partial boundary measurements.

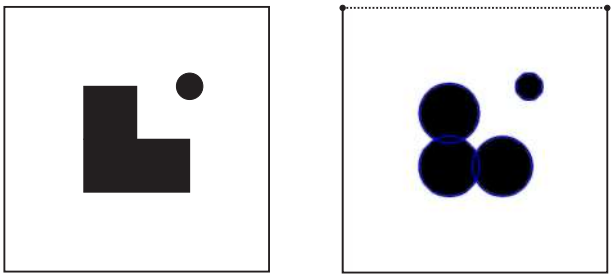

(a) true source term (b) reconstruction

FIGURE 9. Example 5: shape and topology reconstruction.

4.3. **Example 6: Lack of uniqueness.** It is well-known that Problem 1 suffers from lack of uniqueness of solution ω^*. Counter-examples are easy to construct: a body with small support and high density may produce the same traces on Γ_M as another body with larger support and lower density. For instance, in the two-dimensional problem, two concentric circles of same total mass give exactly the same boundary measurements. A ring of same total mass concentric to the circles gives also the same boundary measurements, so that the lack of uniqueness persists even knowing the mass density. In conclusion, even if the intensities γ are known, there is non-uniqueness of the solution ω^*, since different supports ω^* may produce the same boundary data (u^*, q^*). In order to fix these ideas, let us consider three anomalies with different sizes and intensities, whose product between each pair of these quantities leads to the same resulting total mass. The target is shown in Fig. 10(a), where the grayscale represents the intensity of the source. By setting $\gamma = 1$ in the algorithm, we obtain the reconstruction shown in Fig. 10(b). The barycenters and the total mass are perfectly reconstructed, whereas the sizes of two anomalies are missed. In fact, any combination between size and intensity, whose resulting product coincides with the mass of each target, is also solution to this problem. However, if the values of γ are known on different parts of the domain Ω, the real sizes of the anomalies can be promptly obtained, since the total mass of each ball is well estimated.

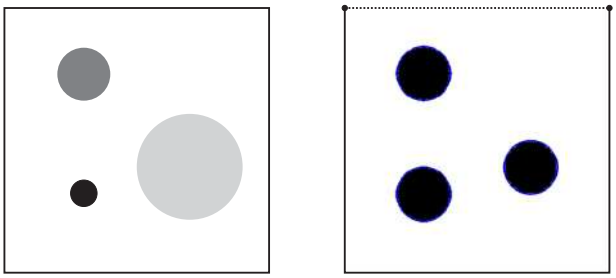

(a) true source term (b) reconstruction

FIGURE 10. Example 6: lack of uniqueness.

4.4. **Examples in three spacial dimensions.** In this section we present some numerical experiments in three dimensions by setting $n = 3$ in the obtained formulas. We use the software package FEniCS for the implementation; see [17] for an introduction. In the examples we take the cube $\Omega = (0,1) \times (0,1) \times (0,1)$ and $\gamma = 1$. The partial boundary measurements are taken on the side of the cube $\Gamma_M = \{x = 1\} \cap \overline{\Omega}$. The domain Ω is discretized using linear Lagrange elements. The mesh is generated from a grid of size $32 \times 32 \times 32$, where each resulting cube is divided into six tetrahedrons, leading to $6 \times 32^3 = 196608$ elements. The subgrid used to evaluate $D^1 J(\widehat{x}_i)$ and $D^2 J(\widehat{x}_i, \widehat{x}_j)$ is set to $10 \times 10 \times 10$ nodes.

4.4.1. *Example 7: three balls, noiseless data.* In this example we aim at reconstructing three balls with centers $(0.7, 0.7, 0.4)$, $(0.6, 0.3, 0.3)$, $(0.5, 0.4, 0.8)$ and with radii 0.17, 0.2, 0.15 respectively.

We use synthetic measurements without noise in the data. The results are given in Table 1. We observe that the algorithm reconstructs the positions of the three balls exactly. The result is shown in Fig. 11. This example shows that the method gives a precise idea of qualitative as well as quantitative features of the real anomalies, such as location, size and even topology.

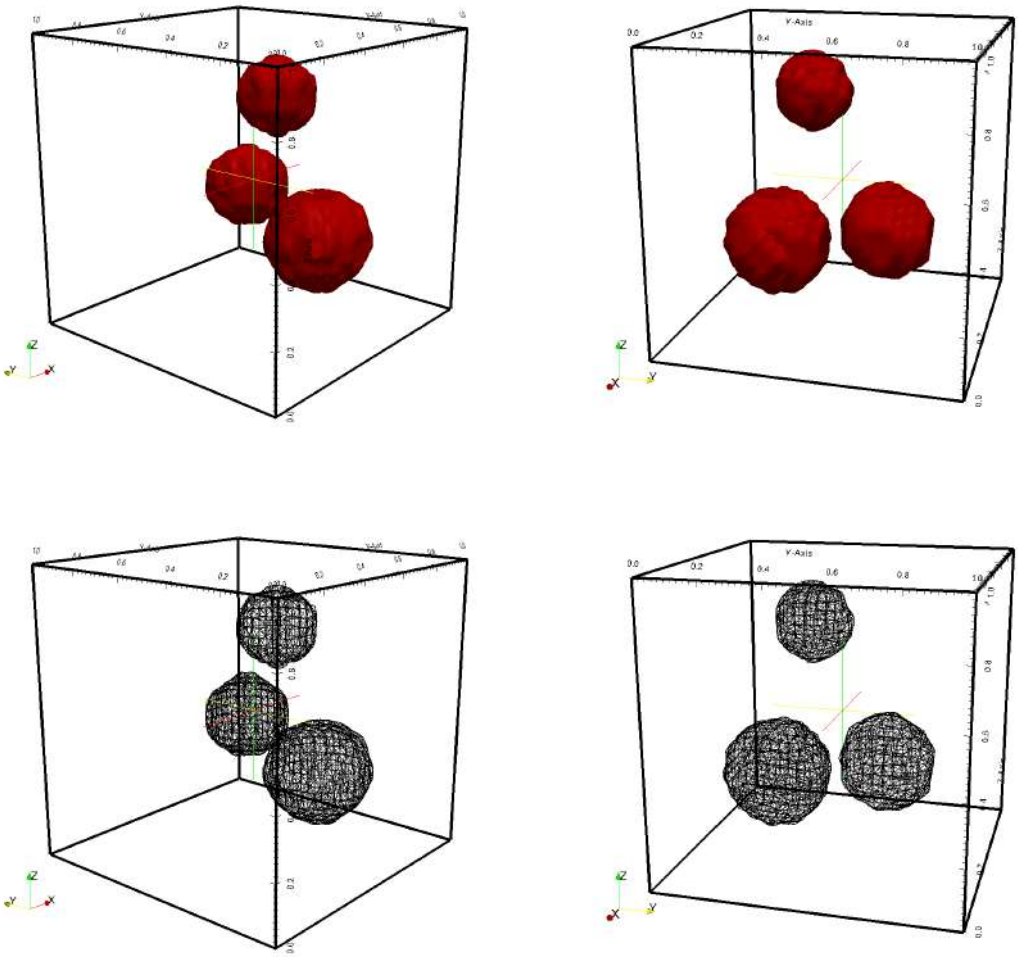

FIGURE 11. Example 7: true anomalies (first row) and corresponding reconstructions (second row).

TABLE 1. Example 7: comparison between the true balls and the reconstruction without noise in 3D; position of the center of the balls and their radii.

	first ball	second ball	third ball
true ball position	$(0.7, 0.7, 0.4)$	$(0.6, 0.3, 0.3)$	$(0.5, 0.4, 0.8)$
reconstructed ball position	$(0.7, 0.7, 0.4)$	$(0.6, 0.3, 0.3)$	$(0.5, 0.4, 0.8)$
true ball radius	0.17	0.2	0.15
reconstructed ball radius	0.171	0.1995	0.151

4.4.2. *Example 8: three balls, noisy data.* In this example we aim at reconstructing three balls with centers $(0.7, 0.7, 0.4)$, $(0.6, 0.3, 0.3)$, $(0.5, 0.4, 0.8)$ and with respective radii 0.17, 0.2, 0.15. In order to obtain noisy synthetic data, the true source term b^* is corrupted with white Gaussian noise, where the resulting level of noise on the boundary measurements is computed as follows:

$$\eta = \frac{\|u^* - u_n^*\|_{L^2(\Gamma_M)} + \|q^* - q_n^*\|_{L^2(\Gamma_M)}}{\|u^*\|_{L^2(\Gamma_M)} + \|q^*\|_{L^2(\Gamma_M)}} \times 100 \,, \tag{4.33}$$

where u_n^* and q_n^* are the noisy boundary measurements used as synthetic data.

In Table 2 and Table 3 results of the reconstruction are shown for $\eta = 0.86\%$ and $\eta = 3.54\%$, respectively. These results correspond to Fig. 12 for Table 2 and Figs. 13-15 for Table 3. One observes that for $\eta = 0.86\%$ the positions are perfectly reconstructed except for the z-coordinate of the third ball, while the radii are also very close to the true value. For $\eta = 3.54\%$ the positions are reasonably well reconstructed. In this case the reconstructed radii shows some deviation but are not too far from the true radii.

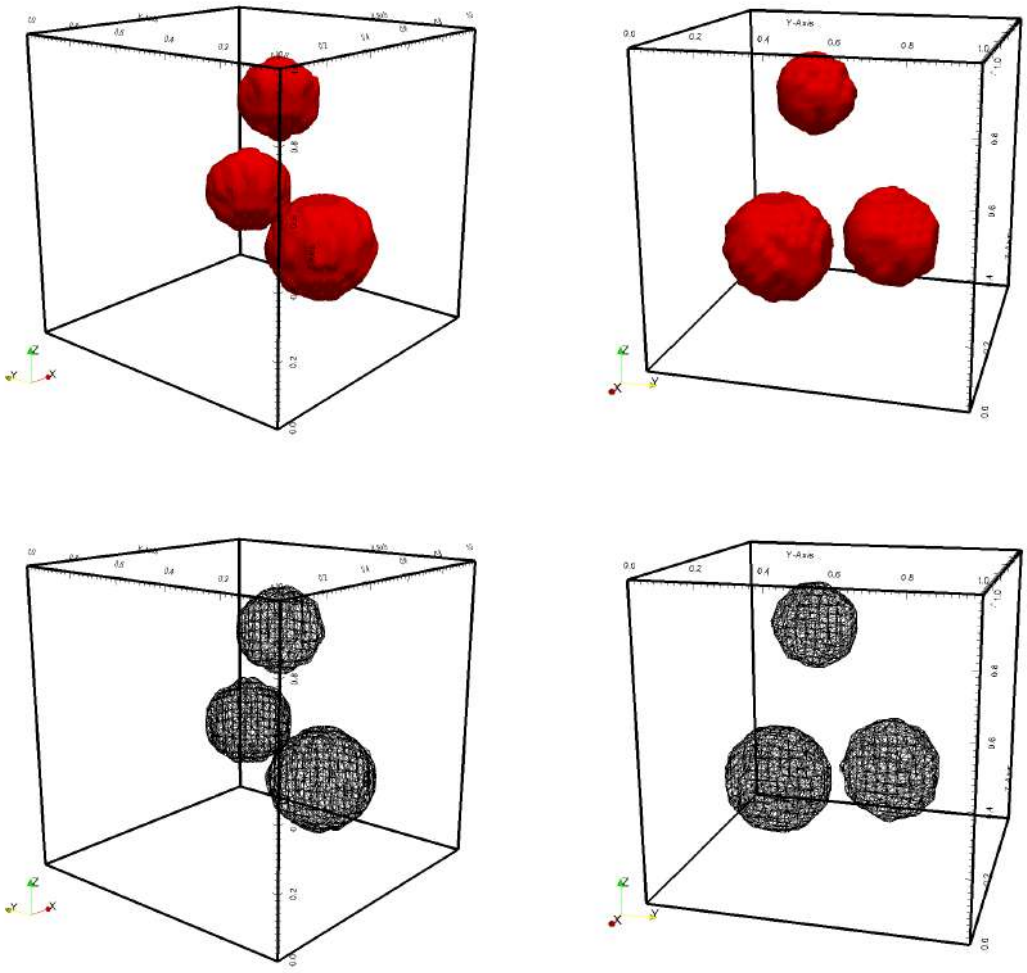

FIGURE 12. Example 8: two different views of true anomalies (first row) and corresponding reconstructions (second row) for $\eta = 0.86\%$.

4.4.3. *Example 9: Two cubes.* In this example we aim at reconstructing two cube-shaped anomalies with centers $(0.6, 0.7, 0.3)$, $(0.4, 0.3, 0.7)$ and with edge length 0.36 without noise in the data. The algorithm reconstructs the two cubes by giving two balls of center $(0.5, 0.7, 0.3)$ and $(0.5, 0.3, 0.7)$ and approximate radii 0.23 and 0.18, respectively. The result is shown in Fig. 16.

TABLE 2. Example 8: comparison between the true balls and the reconstruction with noise; position of the center of the balls and their radii for $\eta = 0.86\%$.

	first ball	second ball	third ball
true ball position	$(0.7, 0.7, 0.4)$	$(0.6, 0.3, 0.3)$	$(0.5, 0.4, 0.8)$
reconstructed ball position	$(0.7, 0.7, 0.4)$	$(0.6, 0.3, 0.3)$	$(0.5, 0.4, 0.8)$
true ball radius	0.17	0.2	0.15
reconstructed ball radius	0.1727	0.1952	0.1566

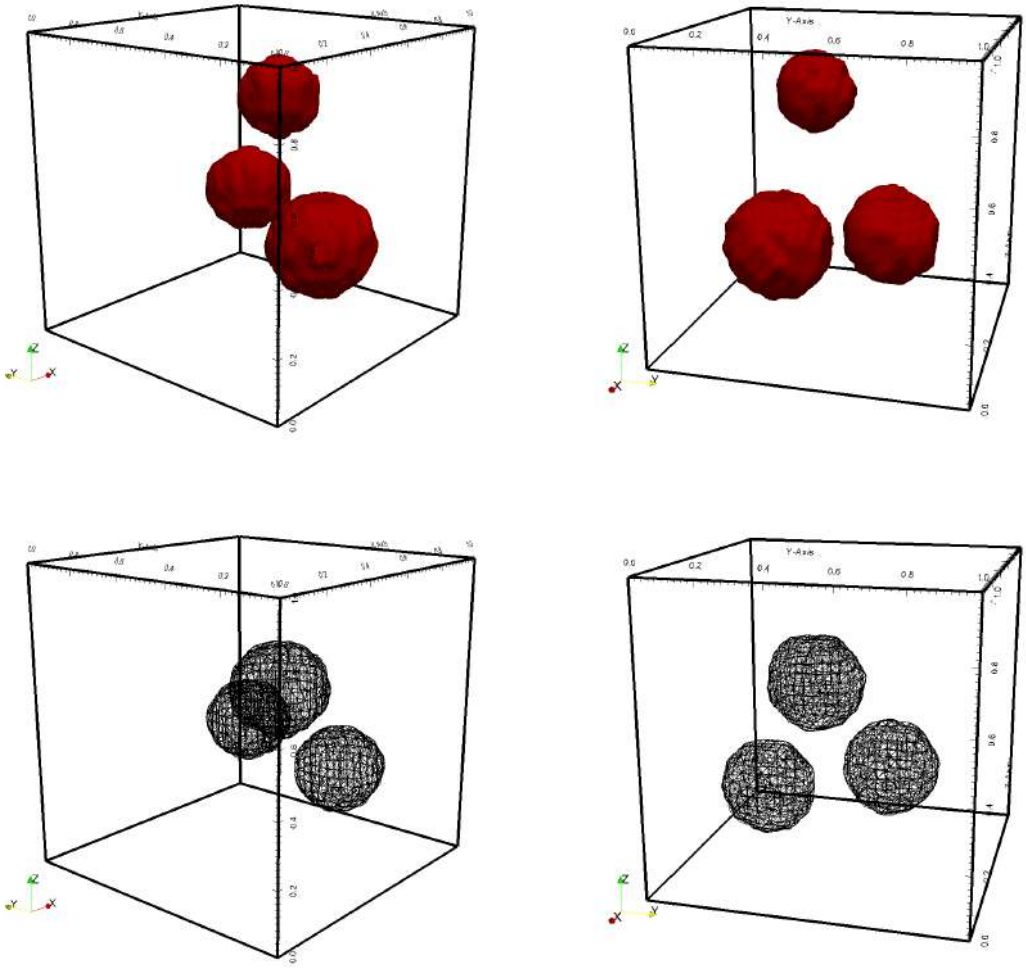

FIGURE 13. Example 8: true anomalies (first row) and corresponding reconstructions (second row) for $\eta = 3.54\%$.

We observe that the two (y, z) coordinates are exactly reconstructed whereas the x-coordinate deviates slightly compared to the true anomalies. The larger ball for the reconstruction is the one closest to the side Γ_M where the measurements are performed. This example shows that the proposed method is able to give a good approximation of the centers and size of two objects whose shapes are not balls and from partial boundary measurements.

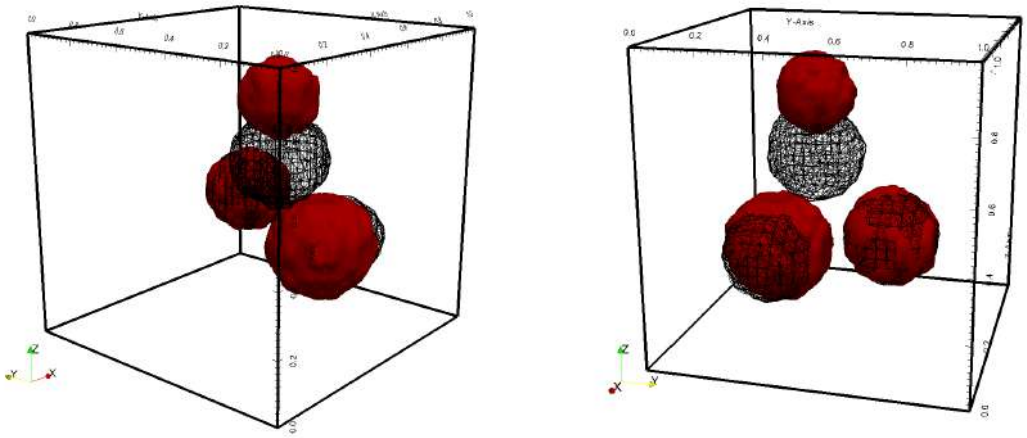

FIGURE 14. Example 8: superposition of true anomalies (red) and corresponding reconstructions (black wireframe) for $\eta = 3.54\%$.

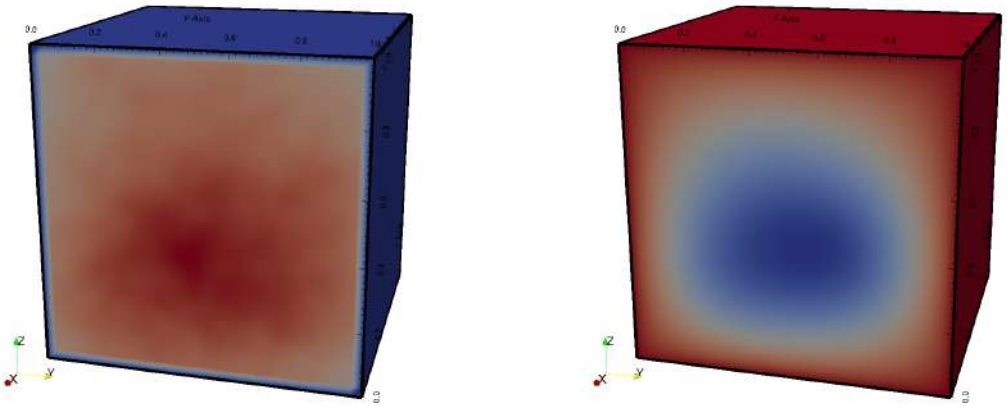

FIGURE 15. Example 8: Solutions u^D (left) and u^N (right) showing the face $\Gamma_M \subset \{x = 1\}$ of the cube where the measurements are performed for $\eta = 3.54\%$.

TABLE 3. Example 8: Comparison between the true balls and the reconstruction with noise; position of the center of the balls and their radii for $\eta = 3.54\%$.

	first ball	second ball	third ball
true ball position	$(0.7, 0.7, 0.4)$	$(0.6, 0.3, 0.3)$	$(0.5, 0.4, 0.8)$
reconstructed ball position	$(0.7, 0.7, 0.4)$	$(0.7, 0.3, 0.3)$	$(0.5, 0.4, 0.6)$
true ball radius	0.17	0.2	0.15
reconstructed ball radius	0.1641	0.1657	0.1775

5. CONCLUSIONS

Following the approach introduced in [7], we have proposed a method for solving two and three-dimensional inverse source problems with partial boundary measurements. The inverse

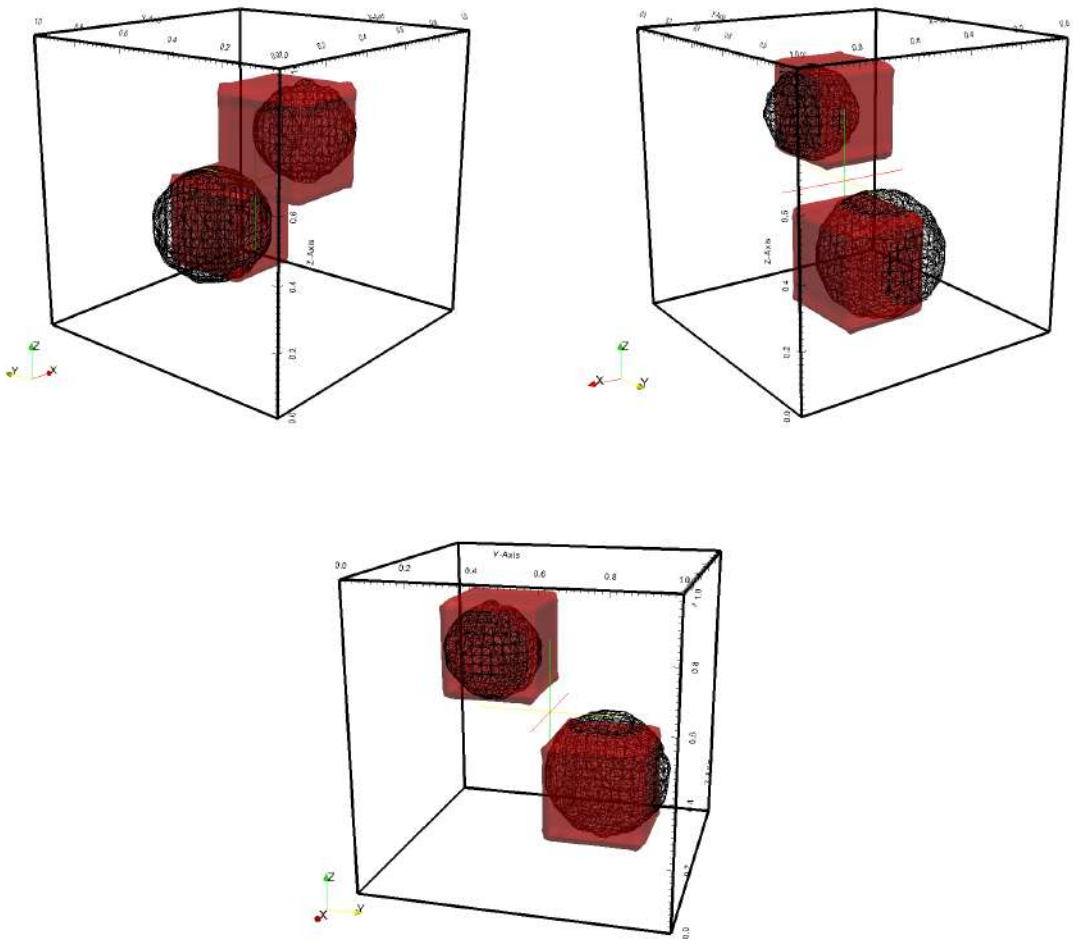

FIGURE 16. Example 9: three different views of true anomalies represented by solid surfaces (two cubes) and corresponding reconstruction represented by a black wireframe (two balls).

source problem have been reformulated as a topology optimization problem, where the support of the mass distribution is the unknown variable and the Kohn-Vogelius functional is minimized. To solve the inverse problem, the algorithm evaluates an analytic formula, herein given, that expresses the variation of the Kohn-Vogelius functional with respect to a set of ball-shaped perturbations on the unknown mass distribution. To complement the unavailable information on the hidden boundary the Newtonian potential was introduced.

By solving some numerical experiments, we have shown that the proposed algorithm is able to approximate the unknown mass distribution in the two and three-dimensional cases and considering different sizes of the hidden boundary and different amounts of noise. The number of unknown anomalies can be found after some trials. The sizes and positions of anomalies with possibly very different sizes can be estimated with acceptable accuracy.

From these promising results, we conclude that the proposed algorithm can be used to perform an initial investigation on the presence of hidden anomalies. In addition, the results provided by our algorithm can be used as an initial guess in level-sets-based methods, for instance.

ACKNOWLEDGMENTS

This research was partly supported by ANII and CSIC (Uruguayan Research Councils), and by CNPq (Brazilian Research Council) and FAPERJ (Research Foundation of the State of Rio de

Janeiro). Antoine Laurain acknowledges financial support by the DFG Research Center Matheon "Mathematics for key technologies" through the MATHEON-Project C37 "Shape/Topology optimization methods for inverse problems". This research was initiated on the occasion of the 2013 edition of the workshop on Partial Differential Equations, Optimal Design and Numerics held at the Benasque Center for Science (Spain). The three authors thank the organizers and the supporting institutions.

References

References

[1] S. Amstutz and H. Andrä. A new algorithm for topology optimization using a level-set method. *Journal of Computational Physics*, 216(2):573–588, 2006.

[2] G. B. Arfken and H. J. Weber. *Mathematical methods for physicists*. Harcourt/Academic Press, Burlington, MA, fifth edition, 2001.

[3] F. Barthelmes. *Untersuchungen zur Approximation des äußeren Gravitationsfeldes der Erde durch Punktmassen mit optimierten Positionen*. Ph.D. Thesis, Vöffentlichungen des Zentralinstituts für Physik der Erde, 92, Potsdam, Germany, 1986.

[4] F. Barthelmes and R. Dietrich. Use of point masses on optimized positions for the approximation of the gravity field. In R. H. Rapp and F. Sansò, editors, *Determination of the Geoid*, volume 106 of *International Association of Geodesy Symposia*, pages 484–493. Springer New York, 1991.

[5] M. S. Bazaraa, H. D. Sherali, and C. M. Shetty. *Nonlinear programming*. Wiley-Interscience [John Wiley & Sons], Hoboken, NJ, third edition, 2006. Theory and algorithms.

[6] M. Burger. A level set method for inverse problems. *Inverse Problems*, 17:1327–1356, 2001.

[7] A. Canelas, A. Laurain, and A. A. Novotny. A new reconstruction method for the inverse potential problem. *Journal of Computational Physics*, 268:417–431, 2014.

[8] S. J. Claessens, W. E. Featherstone, and F. Barthelmes. Experiences with point-mass gravity field modelling in the Perth region, Western Australia. *Geomatics Research Australasia*, 75:53–86, 2001.

[9] M. Hintermüller and A. Laurain. Electrical impedance tomography: from topology to shape. *Control Cybernet.*, 37(4):913–933, 2008.

[10] V. Isakov. *Inverse source problems*, volume 34 of *Mathematical Surveys and Monographs*. American Mathematical Society, Providence, RI, 1990.

[11] V. Isakov. *Inverse problems for partial differential equations*, volume 127 of *Applied Mathematical Sciences*. Springer-Verlag, New York, 1998.

[12] V. Isakov, S. Leung, and J. Qian. A fast local level set method for inverse gravimetry. *Commun. Comput. Phys.*, 10(4):1044–1070, 2011.

[13] R. Kohn and M. Vogelius. Determining conductivity by boundary measurements. *Comm. Pure Appl. Math.*, 37(3):289–298, 1984.

[14] R. Kohn and M. Vogelius. Identification of an unknow conductivity by means of measurements at the boundary. *Inverse Problems*, 14:113–123, 1984.

[15] R. Lehmann. The method of free-positioned point masses – geoid studies on the Gulf of Bothnia. *Bulletin Géodésique*, 67(1):31–40, 1993.

[16] A. Leitão and J. Baumeister. *Topics in Inverse Problems*. IMPA Mathematical Publications, Rio de Janeiro, 2005.

[17] A. Logg, K.-A. Mardal, and G. N. Wells, editors. *Automated Solution of Differential Equations by the Finite Element Method*, volume 84 of *Lecture Notes in Computational Science and Engineering*. Springer, 2012.

[18] A. A. Novotny and J. Sokołowski. *Topological derivatives in shape optimization*. Interaction of Mechanics and Mathematics. Springer, 2013.

[19] J. Shin, J. P. Spicer, and J. A. Abell. Inverse and direct magnetic shaping problems. *Structural and Multidisciplinary Optimization*, 46(2):285–301, 2012.

[20] P. Tricarico. Global gravity inversion of bodies with arbitrary shape. *Geophysical Journal International*, 195(1):260–275, 2013.

(A. Canelas) Instituto de Estructuras y Transporte, Facultad de Ingeniería, Universidad de la República, Av. Julio Herrera y Reissig 565, C.P. 11.300, Montevideo, Uruguay
E-mail address: acanelas@fing.edu.uy

(A. Laurain) Department of Mathematics, Technical University of Berlin, Strasse des 17. Juni 136, 10623 Berlin, Germany
E-mail address: laurain@math.tu-berlin.de

(A.A. Novotny) Laboratório Nacional de Computação Científica LNCC/MCT, Coordenação de Matemática Aplicada e Computacional, Av. Getúlio Vargas 333, 25651-075 Petrópolis - RJ, Brasil
E-mail address: novotny@lncc.br